LES study of the impact of the wake structures on the aerodynamics of a simplified ICE2 train subjected to a side wind

Hassan Hemida[1] and Siniša Krajnović[2]

[1] Division of Fluid Dynamics, Department of Applied Mechanics, Chalmers University, SE-412 96 Gothenburg, SWEDEN hemida@chalmers.se
[2] Division of Fluid Dynamics, Department of Applied Mechanics, Chalmers University, SE-412 96 Gothenburg, SWEDEN sinisa@chalmers.se

1 Introduction

Until recently, experimental studies and numerical simulations of the flow around trains in side winds have focused on measuring the main integral quantities, such as the aerodynamic forces and moments, but not much on understanding the flow structures. Chiu and Squire [1] experimentally found that at low yaw angles (up to 40^o) the flow is similar to the steady slender body flow, in which pairs of steady line vortices are emerging from the separation lines on the lee-side face to form the wake structures. When the side-wind yaw angle increases above 60^o, the flow changes from that associated with a slender body to unsteady vortex shedding. However, the mechanism of this transition between these two types of flows and its effect on the aerodynamic forces have not been investigated in detail. The present investigation focuses on the impact of the wake structures on the aerodynamic coefficients by solving the flow around a simplified ICE2 train subjected to a 30^o side-wind yaw angle using large-eddy simulation (LES). Standard Smagorinsky model with a model constant $C_s = 0.1$ is used to model the subgrid scales. The Reynolds number is 2×10^5, based on the freestream velocity and the height of the train, D. The simplified train model consists of a leading car to which an end car dummy is attached (see Fig. 1b). The total length of the train model is $L = 3.552m$ and its height is $D = 0.358m$. The clearance between the train and the computational domain floor is $0.0537m$ $(0.15D)$. The LES results are compared with wind tunnel test results. The measurements were made in the subsonic Russian $TsAGI\ T-103$ open jet tunnel. The experimental set-up is shown in Fig. 1a. In contrast to the computational model, the wind tunnel model has bogies and an inner gap between the leading car and the dummy end car. The model stands on a thin elliptic plate (see Fig. 1a) to reduce the thickness of the approaching boundary layer. Moreover, in order to keep the

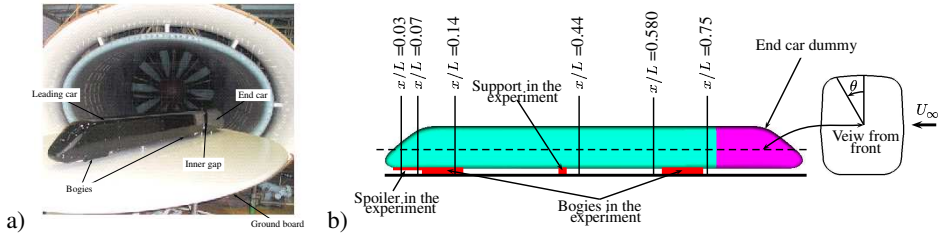

Fig. 1. (a) Experimental set-up, (b) simplified model.

ground clearance, the model is held by a single cylindrical support positioned midway between the bogies. To simplify the model in the computations, the inner gap is filled and both the bogies and the cylindrical support are removed. In the measurements, the Reynolds number was $Re = 1.4 \times 10^6$ based on the free-stream velocity and the height of the train. In the computational domain, the model is yawed 30^o to the free-stream direction as shown in Fig. 2. The clearance between the model and the ground board is the same as in the experimental set-up. The model centerline is kept parallel to the inlet of the domain with a streamwise distance of $8D$ to ensure the same thickness of the approaching boundary layer. The distance between the train tail and the exit of the computational domain is $21D$. The height of the computational domain is $5.2D$. The flow enters the domain with a uniform velocity profile

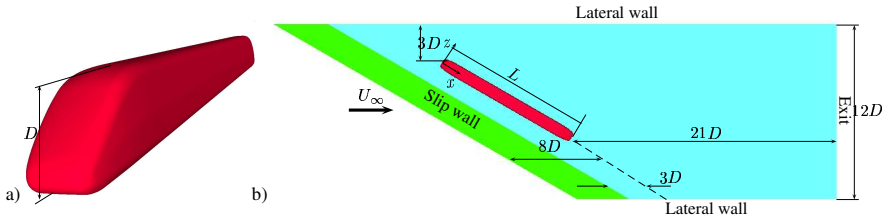

Fig. 2. The computational domain.

constant in time. A convective-velocity boundary condition is implemented at the domain exit. No-slip boundary conditions are used on the train surface. To simulate the experimental set-up, a slip boundary condition is applied at the lateral walls and the roof. To reduce the thickness of the boundary layer approaching the train model, two kinds of boundary conditions are applied at the channel floor. A slip boundary condition is applied on a part extending $5D$ (see Fig. 2b) from the inlet to suppress the development of a boundary layer, while a no-slip boundary condition is used on the rest of the floor. A homogeneous Neumann boundary condition is used for the pressure on all the boundaries.

2 Results

Numerical accuracy is investigated by performing two simulations with different number of nodes: 6 and 12 million nodes. The spatial resolutions of the first cell layer at the model and floor are shown in Table 1 for the two meshes, where u^* is the friction velocity, n is the distance between the first node and the train surface in the wall normal direction, Δs is the cell width in the streamwise direction and Δl is the cell width in the span-wise direction.

Table 1. Spatial resolutions for the coarse and the fine mesh simulations.

		$y^+ = nu^*/\nu$	$s^+ = \Delta s u^*/\nu$	$l^+ = \Delta l u^*/\nu$
fine	mean	0.5	40	90
	maximum	4	250	700
coarse	mean	1.5	100	300
	maximum	20	450	1200

The surface pressure distributions are computed at certain cross-sections along the length of the train where experimental data are available, as shown in Fig. 1b. Figure 1b also shows some details from the experimental train, such as spoiler, support, bogies and inner-car gap, which are omitted from the computational model. These differences should be kept in mind when comparing the LES results with the experimental data. Figure 3 shows the local pressure coefficient, C_p, over the circumferential angle, θ, measured counterclockwise around the x-axis, as shown in Fig. 1b. Although the LES results from the coarse and fine meshes are found to be in a good agreement with the experimental data on the nose of the train ($x/L < 0.14$), the coarse mesh simulation was not able to obtain the minimum pressure on the top and bottom-side faces as shown in Fig. 3. Far from the nose of the train, the resolution of the coarse mesh is not sufficient to get results that agree with the experimental data, especially on the bottom and top-side faces. The LES results from the fine mesh show good agreement with the measurements on the streamwise and top-side faces at all the cross-sections. Moreover, good correlation is obtained between the LES results from the fine mesh and the measured data on the lee-side face. The difference in the geometry under the train (i.e. bogies, the spoiler and the support) between the experimental and the numerical set-ups resulted in a difference in C_p values on the surface of the under side. The effect of these complexities is believed to be localized since it does not influence the pressure on the other faces. The maximum suction peak and the highest pressure are found on the upper-face leeward edge of the nose and on the streamwise face of the nose, respectively, at two front cross-sections, $x/L = 0.03$ and $x/L = 0.07$ (Fig. 3). The peak C_p magnitudes in these two sections are almost twice as large as those in the subsequent cross-sections. This suggests that the loads are accumulated in the nose region of the leading

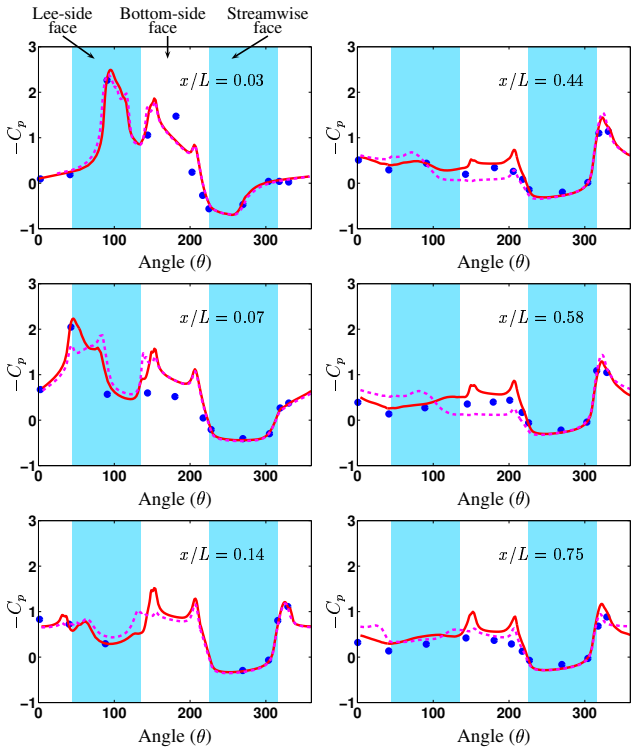

Fig. 3. Time-averaged surface pressure: (solid) fine mesh, (dashed) coarse mesh, (symbols) experimental data.

car. In general, although the LES Reynolds number is seven times lower than the experimental one, the LES results are in fairly good agreement with the measurements.

Figure 4 shows the LES wake structures by means of isosurface of the instantaneous pressure. The flow separates from the top-side face at the windward edge. It reattaches to the surface forming small separation bubble on the top side face. On the other side, the flow remains attached to the bottom-side face before it enters the wake. Both of the flows on the bottom-side and top-side faces separate from the surface when they reach the lee-side face to form line vortices emerging from the separation lines. These line vortices are forming the wake flow patterns. The upper vortices are stronger and more steady than the lower-side ones. Figure 4 shows that the first upper vortex stretches in the wake flow all the way from the nose tip to the end of the leading car. It grows in size but remains attached to the train surface. It is steady for a length of about $5D$ from its onset at the front of the train before it becomes unsteady and breaks up. The lower vortices are highly unsteady. The cores of these vortices oscillate in a horizontal plan with low frequencies,

where they attach and detach to and from the surface of the train with the same frequency. The vortex shedding in the wake is mainly from the lower vortices. Attachment and detachment of the wake vortices to the train leave disturbances on its surface pressure which affect the aerodynamic coefficients. Our LES resulted in wake structures are in agreement with those obtained

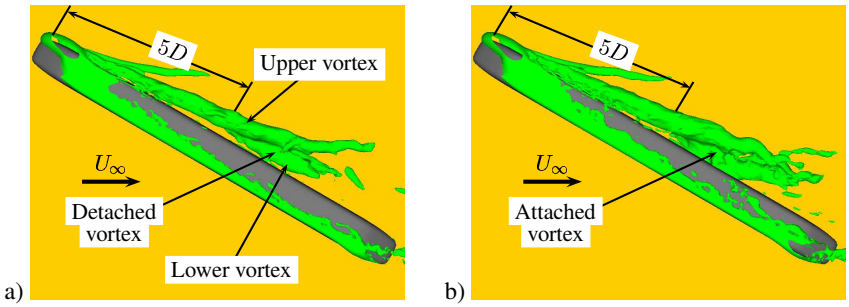

Fig. 4. Isosurface of the instantaneous pressure $p = -0.4Pa$ at two different times.View is from above the train.

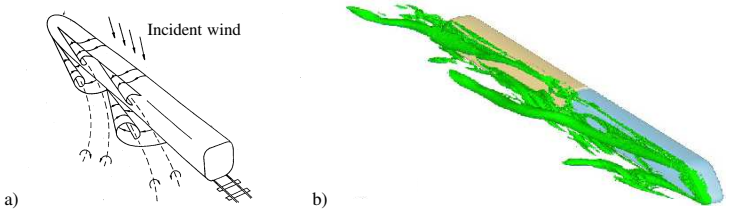

Fig. 5. (a) Experimental view (taken from [2]). (b) DES results (taken from [3]).

by Wu [3] using Detached-Eddy Simulation (see Fig. 5b). On contrary to our finding, Copley [2] reported that the lower-side vortices of the wake are mirror images of the upper-side ones. They found that these vortices are shed from successive points along the train length with the same vortex strength to form a three-dimensional Von Karmen Vortex Street (see Fig. 5a).

The time histories of the side force and the lift force coefficients, C_s and C_l, are shown in Figs. 6a and 6b, respectively. In order to find the frequencies of the different motions in the flow, the power spectra of the aerodynamic coefficients are drawn against the Strouhal number, St, as shown in Figs. 6c and 6d. The major peak in the spectra is corresponding to the attachment and detachment of the wake vortices to and from the surface of the train. The second dominating frequencies are corresponding to the shedding frequencies.

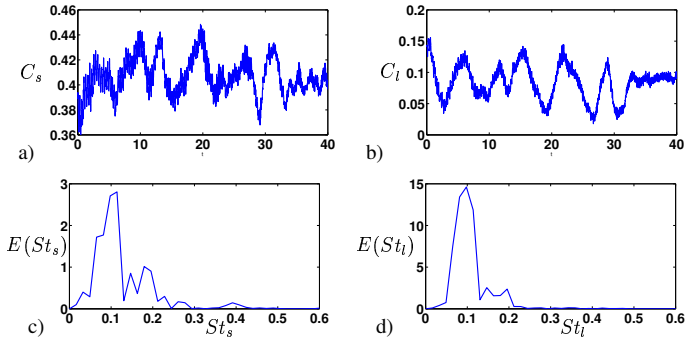

Fig. 6. (a) and (b) are time history of the side force and the lift force coefficients, C_l and C_s, respectively. (c) and (d) are the corresponding autopower spectra.

To conclude, the present work shows that LES is capable of accurately predicting the flow around a high-speed train such as ICE2. Our LES have provided a new picture to the wake flow that differs from the previously published experimental picture.

3 Acknowledgments

This work was supported by the Swedish Agency for Innovation System (VINNOVA), Bombardier Transportation, and Scania. Computer time on HPC2N (High Performance Computing Center North), NSC (National Supercomputer Center in Sweden), HIVE supercomputer at SWEGRID, and the HELIOS supercomputer provided by UNICC at Chalmers are gratefully acknowledged.

References

1. T. W. Chiu and L. C. Squire. An experimental study of the flow over a train in a crosswind at large yaw angles up to 90°. *Journal of Wind Engineering and Industrial Aerodynamics*, 45:47–74, 1992.
2. J. M. Copley. The three-dimensional flow around railway trains. *Journal of Wind Engineering and Industrial Aerodynamics*, 26:21–52, 1987.
3. D. Wu. Predictive prospects of unsteady detached-eddy simulations in industrial external aerodynamic flow simulations. Diploma thesis. matriculation number: 219949, Lehrstuhl fur Strmungslehre und Aerodynamishes Institute, Aachen, Germany, 2004.